

# Magic wavelengths of $\text{Ca}^+$ ion for linearly and circularly polarized light

Jun Jiang,\* Li Jiang, Xia Wang, Deng-Hong Zhang, Lu-You Xie, and Chen-Zhong Dong  
 Key Laboratory of Atomic and Molecular Physics and Functional Materials of Gansu Province,  
 College of Physics and Electronic Engineering, Northwest Normal University, Lanzhou 730070, P. R. China  
 (Dated: March 30, 2017)

The dynamic dipole polarizabilities of the low-lying states of  $\text{Ca}^+$  for linearly and circularly polarized light are calculated by using relativistic configuration interaction plus core polarization (RCICP) approach. The magic wavelengths, at which the two levels of the transitions have the same ac Stark shifts, for  $4s-4p_{j,m}$  and  $4s-3d_{j,m}$  magnetic sublevels transitions are determined. The present magic wavelengths for linearly polarized light agree with the available results excellently. The polarizability for the circularly polarized light has the scalar, vector and tensor components. The dynamic polarizability is different for each of magnetic sublevels of the atomic state. Additional magic wavelengths have been found for the circularly polarized light. We recommend that the measurement of the magic wavelength near 850 nm for  $4s-4p_{\frac{3}{2},m=\pm\frac{3}{2},\pm\frac{1}{2}}$  could be able to determine the oscillator strength ratio of  $f_{4p_{\frac{3}{2}}\rightarrow 3d_{\frac{3}{2}}}$  and  $f_{4p_{\frac{3}{2}}\rightarrow 3d_{\frac{5}{2}}}$ .

PACS numbers: 31.15.ac, 31.15.ap, 34.20.Cf

## I. INTRODUCTION

The magic wavelength, at which the ac Stark shift of the transition energy is zero for the certain frequencies, was introduced in Refs.[1, 2]. The magic wavelengths have been extensively used in ultraprecise optical lattice clocks[3–9], the state-insensitive quantum engineering [10, 11].

The magic wavelengths for the linearly polarized light have been studied for alkali-metal and alkaline-earth-metal atoms in experiment and theory[12–18]. The magic wavelengths of alkali-metal atoms for the circularly polarized light have been calculated[10, 19–21]. The use of circularly polarized light has advantages owing to the vector polarizabilities which are absent in the linearly polarized light, such as magnetic-sublevel selective trapping and far-off-resonance laser trapping[10, 22].

$\text{Ca}^+$  is an alkali-metal like ion. Since the nuclear spin is zero for  $^{40}\text{Ca}^+$ , it is immune to the first-order Zeeman frequency shift[23] and convenient for laser cooling. The  $^{40}\text{Ca}^+$  ion is preferred for optical frequency standard and quantum computing[24–28]. The frequency of  $^{40}\text{Ca}^+$  optical clocks has been measured with an uncertainty at the  $10^{-17}$  level [29].

Recently, two magic wavelengths of the  $^{40}\text{Ca}^+$   $4s-3d_{\frac{5}{2},m=\frac{1}{2},\frac{3}{2}}$  clock transitions for the linearly polarized light are measured with very high precision [14]. This measurement agrees with the theoretical predictions of B-spline Dirac-Fock plus core polarization (DFCP) method [15] excellently. Meanwhile, the measurement for these two magic wavelengths determines the ratio of  $4s-4p_{\frac{1}{2}}$  and  $4s-4p_{\frac{3}{2}}$  oscillator strength with the deviation less than 0.5%.

In this paper, the energy levels, electric dipole matrix

elements and static polarizabilities are calculated using relativistic configuration interaction plus core polarization (RCICP) method. The dynamic dipole polarizabilities of the  $4s$ ,  $4p_j$  and  $3d_j$  states of  $\text{Ca}^+$  ion are calculated for the linearly and circularly polarized light. The magic wavelengths for each of magnetic sublevel transitions are determined. In Sec. II., a brief description of the theoretical method is presented. In Sec. III., the static and dynamic polarizabilities and magic wavelengths are discussed. In Sec. IV., a few conclusions are pointed out. The unit used in the present calculations is atomic unit (a.u.).

## II. THEORETICAL METHOD

The energy levels and transition arrays are calculated using RCICP method which has been developed recently [39]. The present method is similar to the calculation of magic wavelengths of  $\text{Ca}^+$  for the linearly polarized light by Tang *et al.* [15], except that they use the B-spline basis. The basic strategy of the model is to partition the atom into valence and core electrons. The first step involves a Dirac-Fock (DF) calculation of the  $\text{Ca}^{2+}$  ground state. The orbitals of the core are written as linear combinations of S-spinors which can be treated as relativistic generalizations of the Slater-type orbitals.

Then, the effective interaction of the valence electron with the core is written as

$$H = c\boldsymbol{\alpha} \cdot \mathbf{p} + \beta c^2 + V_{\text{core}}(\mathbf{r}). \quad (1)$$

The core operator is

$$V_{\text{core}}(\mathbf{r}) = -\frac{Z}{r} + V_{\text{dir}}(\mathbf{r}) + V_{\text{exc}}(\mathbf{r}) + V_p(\mathbf{r}), \quad (2)$$

where  $V_{\text{dir}}$ ,  $V_{\text{exp}}$  are direct and exchange interactions with core electrons. The semi-empirical core polarization potential is introduced to approximate the correlation interaction between the core and valence electrons.

\*Electronic address: phyjiang@yeah.net

TABLE I: Relativistic dipole polarizabilities (a.u.) of the ground and low-lying excited states of  $\text{Ca}^+$  ion. The numbers in parentheses are uncertainties by introducing 0.5% uncertainties into the dominant matrix elements.

	$4s_{\frac{1}{2}}$	$3d_{\frac{3}{2}}$		$3d_{\frac{5}{2}}$		$4p_{\frac{1}{2}}$	$4p_{\frac{3}{2}}$	
	$\alpha_1$	$\alpha_1$	$\alpha_1^t$	$\alpha_1$	$\alpha_1^t$	$\alpha_1$	$\alpha_1$	$\alpha_1^t$
	Dipole							
Present	75.46(72)	32.98(24)	-17.97(17)	32.80(24)	-25.28(24)	-2.98(11)	-1.12(10)	10.20(11)
DFCP [15]	75.28	32.99	-17.88	32.81	-25.16	-2.774	-0.931	10.12
MBPT-SD [30]	76.1(5)	32.0	-17.43(23)	32.0	-24.51(29)	-0.75	1.02(64)	10.31(28)
CICP [31]	75.49	32.73	-17.64	32.73	-25.20	-2.032	-2.032	10.47
RCC [32]	73.0(1.5)	28.5(1.5)	-15.87	29.5(1.0)	-22.49(5)			
RCC-STO [32]	74.3	31.6	-17.7	32.5	-25.5			
f-sums[33]	75.3(4)							

TABLE II: Comparison of static scalar polarizabilities (a.u.) for  $4s_{\frac{1}{2}}$  and  $3d_{\frac{5}{2}}$  states and blackbody radiation shift (Hz) for the  $4s_{\frac{1}{2}} - 3d_{\frac{5}{2}}$  transition of  $^{40}\text{Ca}^+$  ion at  $T=300$  K.

	Present	Ref.[31]	Ref.[32]	Ref.[17]	Ref.[34]	Ref.[35]	Expt.[36]	Ref.[37, 38]
$\alpha_0(4s_{\frac{1}{2}})$	75.46(72)	75.49	73.0(1.5)	76.1(1.1)	76	73	76.1(1.1)	
$\alpha_0(3d_{\frac{5}{2}})$	32.80(24)	32.73	29.5(1.0)	32.0(1.1)	31	23	31.8(3)	
$\Delta\alpha$	42.66	42.76	43.5	44.1	45	40	44.3	
$\eta(4s_{\frac{1}{2}})$	-3.0[-9]							
$\eta(3d_{\frac{5}{2}})$	-1.1[-8]							
BBR shift	0.367(39)	0.368	0.37(1)	0.38(1)	0.39(27)	0.4	0.35(0.009) <sup>a</sup>	0.35

<sup>a</sup>The temperature is 294.4 K in this experiment.

The  $\ell$ -dependent polarization potential  $V_p$  can be written as

$$V_p(r) = \sum_{\ell m} \frac{\alpha g_{\ell}^2(r)}{2r^4} |\ell m\rangle \langle \ell m|, \quad (3)$$

$\alpha$  is the static dipole polarizability of the core,  $\alpha = 3.26$  a.u.[40] and  $g_{\ell}^2(r)$  is a cutoff function,  $g_{\ell}^2(r) = 1 - \exp(-r^6/\rho_{\ell}^6)$ .  $\rho_{\ell}$  is an adjustable parameter that is tuned to reproduce the binding energies of the corresponding states. The orbitals of the valence electron are written as linear combinations of L-spinors and S-spinors. L-spinors can be treated as relativistic generalizations of the Laguerre-type orbitals. See Supplemental Tables I and II for lists of energy levels and electric-dipole matrix elements for some low-lying excited states transitions of  $\text{Ca}^+$  ions [41].

For arbitrary polarized light, the dynamic polarizability  $\alpha_i(\omega)$  is given by [22, 42, 43]

$$\begin{aligned} \alpha_i(\omega) = & \alpha_i^0(\omega) + A \cos\theta_k \frac{m_{j_i}}{2j_i} \alpha_i^1(\omega) \\ & + \left( \frac{3\cos^2\theta_p - 1}{2} \right) \frac{3m_{j_i}^2 - j_i(j_i + 1)}{j_i(2j_i - 1)} \alpha_i^2(\omega), \quad (4) \end{aligned}$$

where  $\alpha_i^0(\omega)$ ,  $\alpha_i^1(\omega)$ ,  $\alpha_i^2(\omega)$  are the scalar, vector, and tensor polarizabilities for state  $i$ , respectively;  $j, m_{j_i}$  are the total angular momentum and the corresponding magnetic quantum number.  $\theta_k$  is the angle between the wave vector of the electric field and  $z$ -axis.  $\theta_p$  relates to the direction of polarization vector and quantization axis which

was defined in Ref.[22, 42]. From geometrical considerations, it is found that  $\theta_k$  and  $\theta_p$  must satisfy the inequality  $\cos^2\theta_k + \cos^2\theta_p \leq 1$ .  $A$  represents the degree of polarization, which can be taken arbitrary value from  $-1$  to  $1$ . For the linearly polarized light,  $A$  is equal to zero. The direction of  $z$ -axis is polarization direction which is perpendicular to the wave vector of the electric field,  $\cos\theta_k = 0$  and  $\cos\theta_p = 1$ .

$$\alpha_i(\omega) = \alpha_i^0(\omega) + \frac{3m_{j_i}^2 - j_i(j_i + 1)}{j_i(2j_i - 1)} \alpha_i^2(\omega). \quad (5)$$

$A = 1$  is for the right handed and  $A = -1$  is for the left handed circularly polarized light. Here, we can choose the direction of  $z$ -axis as the wave vector of the electric field and then  $\cos\theta_k = 1$ ,  $\cos^2\theta_p = 0$ . Then the eq.(4) can be simplified as

$$\alpha_i(\omega) = \alpha_i^0(\omega) + A \frac{m_{j_i}}{2j_i} \alpha_i^1(\omega) - \frac{3m_{j_i}^2 - j_i(j_i + 1)}{2j_i(2j_i - 1)} \alpha_i^2(\omega). \quad (6)$$

The scalar polarizability was conventionally expressed as

$$\begin{aligned} \alpha_i^0(\omega) = & \frac{1}{3(2j_i + 1)} \sum_{in} |\langle \psi_i || D || \psi_n \rangle|^2 \\ & \times \left[ \frac{1}{\Delta E_{in} + \omega} + \frac{1}{\Delta E_{in} - \omega} \right]. \quad (7) \end{aligned}$$

TABLE III: Magic wavelengths (in nm) for the transitions of low-lying states of  $\text{Ca}^+$  for the linearly polarized light. The numbers in the parentheses are uncertainties calculated by assuming certain matrix elements have  $\pm 2\%$  uncertainties.

Resonance Transitions	$\lambda_{res}$	Present	Ref.[13]	Ref.[15]	Exp.[14]
$4s_{\frac{1}{2}} - 4p_{\frac{1}{2}}$					
$4p_{\frac{1}{2}} - 3d_{\frac{3}{2}}$	866.214				
		691.24(12.29)	697.65	690.817(11.984)	
$4p_{\frac{1}{2}} - 4s_{\frac{1}{2}}$	396.847				
		395.1788(377)	395.18	395.1807(14)	
$4p_{\frac{1}{2}} - 5s_{\frac{1}{2}}$	370.603				
		368.0221(1412)	368.10	368.0149(901)	
$4p_{\frac{1}{2}} - 4d_{\frac{3}{2}}$	315.887				
$4s_{\frac{1}{2}} - 4p_{\frac{3}{2}}, m = \frac{3}{2}$					
$4p_{\frac{3}{2}} - 3d_{\frac{5}{2}}$	854.209				
		850.9217(15)	850.12		
$4p_{\frac{3}{2}} - 3d_{\frac{3}{2}}$	849.802				
		672.89(15.33)	678.35	672.508(11.3150)	
$4p_{\frac{1}{2}} - 4s_{\frac{1}{2}}$	396.847				
		395.7729(19)	395.77	395.774(10)	
$4p_{\frac{3}{2}} - 4s_{\frac{1}{2}}$	393.366				
$4s_{\frac{1}{2}} - 4p_{\frac{3}{2}}, m = \frac{1}{2}$					
$4p_{\frac{3}{2}} - 3d_{\frac{5}{2}}$	854.209				
		850.1164(1)	850.12		
$4p_{\frac{3}{2}} - 3d_{\frac{3}{2}}$	849.802				
		687.51(10.33)	693.76	687.022(12.285)	
$4p_{\frac{1}{2}} - 4s_{\frac{1}{2}}$	396.847				
		396.2297(218)	396.23	396.2315(13)	
$4p_{\frac{3}{2}} - 4s_{\frac{1}{2}}$	393.366				
$4p_{\frac{3}{2}} - 5s_{\frac{1}{2}}$	373.690				
		369.6523(1849)	369.72	369.6393(1534)	
$4p_{\frac{3}{2}} - 4d_{\frac{3}{2}}$	318.128				
$4s_{\frac{1}{2}} - 3d_{\frac{3}{2}}, m = \frac{3}{2}$					
		887.28(3.52)	884.54	887.382(3.196)	
$3d_{\frac{3}{2}} - 4p_{\frac{1}{2}}$	866.214				
$4s_{\frac{1}{2}} - 4p_{\frac{1}{2}}$	396.847				
		395.7951 (1)	395.79	395.7970(1)	
$4s_{\frac{1}{2}} - 4p_{\frac{3}{2}}$	393.366				
$4s_{\frac{1}{2}} - 3d_{\frac{3}{2}}, m = \frac{1}{2}$					
		1307.60(96.2)	1252.44	1308.590(71.108)	
$3d_{\frac{3}{2}} - 4p_{\frac{1}{2}}$	866.214				
		850.3301(18)	850.33	850.335(2)	
$3d_{\frac{3}{2}} - 4p_{\frac{3}{2}}$	849.802				
$4s_{\frac{1}{2}} - 4p_{\frac{1}{2}}$	396.847				
		395.7962(1)	395.80	395.7981(1)	
$4s_{\frac{1}{2}} - 4p_{\frac{3}{2}}$	393.366				
$4s_{\frac{1}{2}} - 3d_{\frac{5}{2}}, m = \frac{5}{2}$					
$4s_{\frac{1}{2}} - 4p_{\frac{1}{2}}$	396.847				
		395.7949(1)	395.79	395.7968(1)	
$4s_{\frac{1}{2}} - 4p_{\frac{3}{2}}$	393.366				
$4s_{\frac{1}{2}} - 3d_{\frac{5}{2}}, m = \frac{3}{2}$					
		1073.80(31.61)	1052.26	1074.336(26.352)	
$3d_{\frac{5}{2}} - 4p_{\frac{3}{2}}$	854.209				
$4s_{\frac{1}{2}} - 4p_{\frac{1}{2}}$	396.847				
		395.7958(1)	395.79	395.7978(1)	395.7992(2)
$4s_{\frac{1}{2}} - 4p_{\frac{3}{2}}$	393.366				
$4s_{\frac{1}{2}} - 3d_{\frac{5}{2}}, m = \frac{1}{2}$					
		1337.30(115.38)	1271.92	1338.474(82.593)	
$3d_{\frac{5}{2}} - 4p_{\frac{3}{2}}$	854.209				
$4s_{\frac{1}{2}} - 4p_{\frac{1}{2}}$	396.847				
		395.7963(1)	395.79	395.7982(1)	395.7990(2)
$4s_{\frac{1}{2}} - 4p_{\frac{3}{2}}$	393.366				

The vector polarizability was written as

$$\begin{aligned} \alpha_i^1(\omega) = & -\sqrt{\frac{6j_i}{(j_i+1)(2j_i+1)}} \sum_{in} \left\{ \begin{matrix} j_i & 1 & j_n \\ 1 & j_i & 1 \end{matrix} \right\} \\ & \times (-1)^{j_i+j_n+1} |\langle \psi_i || D || \psi_n \rangle|^2 \\ & \times \left[ \frac{1}{\Delta E_{in} + \omega} - \frac{1}{\Delta E_{in} - \omega} \right]. \end{aligned} \quad (8)$$

The tensor polarizability was expressed as

$$\begin{aligned} \alpha_i^2(\omega) = & -2\sqrt{\frac{5j_i(2j_i-1)}{(6(j_i+1)(2j_i+1)(2j_i+3))}} \\ & \times \sum_{in} \left\{ \begin{matrix} j_i & 1 & j_n \\ 1 & j_i & 2 \end{matrix} \right\} (-1)^{j_i+j_n+1} |\langle \psi_i || D || \psi_n \rangle|^2 \\ & \times \left[ \frac{1}{\Delta E_{in} + \omega} + \frac{1}{\Delta E_{in} - \omega} \right]. \end{aligned} \quad (9)$$

where  $|\langle \psi_i || D || \psi_n \rangle|$  and  $\Delta E_{in}$  are reduced matrix element and excitation energy of transition respectively. For the state with  $j < \frac{1}{2}$ , the tensor polarizability makes no contribution to total polarizability.

### III. POLARIZABILITIES

#### A. STATIC POLARIZABILITIES

When the frequency of light is zero, the dynamic polarizability becomes static dipole polarizability, in which the contribution of vector polarizability is zero. Table I lists dipole scalar and tensor static polarizabilities of the low-lying states of  $\text{Ca}^+$ , which are compared with the available theoretical and experimental results.

For the ground state, the present polarizabilities are in good agreement with the previous calculations[15, 30, 31, 33]. The errors are within 0.8% except for the value calculated by relativistic coupled cluster (RCC) method. There is a significant difference between the values of RCC and other calculations. The scalar and tensor polarizabilities of the  $3d_j$  states are excellently agree with the results of Tang *et al.* [15]. The scalar polarizabilities for the  $4p_j$  states are negative which are caused by the downward transitions to the lower states.

#### B. BLACKBODY RADIATION SHIFT

The accuracy of optical frequency standards is limited by the frequency shift in the clock transitions caused by the interactions of the ion with external field. The major contributions to the systematic frequency shifts come from blackbody radiation (BBR) shift. The frequency shift for a state due to blackbody radiation at temperature  $T$  can be written as

$$\Delta\nu = -\frac{1}{2}(831.9V/m)^2 \left(\frac{T(K)}{300}\right)^4 \alpha_i^0(1+\eta), \quad (10)$$

where  $\alpha_i^0$  is the static scalar polarizability for state  $i$ . The factor  $\eta$  is a small dynamic correction [44],

$$\begin{aligned} \eta = & \frac{(80/63)\pi^2}{\alpha_n^{(E1)}(0)T} \sum_i \frac{|\langle \psi_i || D || \psi_n \rangle|^2}{(2J_n+1)y_i^3} \\ & \times \left(1 + \frac{21\pi^2}{5y_i^2} + \frac{336\pi^4}{11y_i^4}\right). \end{aligned} \quad (11)$$

As Table II shows the value of  $\eta$  can be negligible. Here  $y_i = \omega_{in}/T$  and  $T$  is temperature, we set as 300 K. The atomic unit for  $\alpha$  can be converted to SI units via  $\alpha/h[H\text{z}/(V/m)^2] = 2.48832 \times 10^{-8} \alpha[a.u.]$ .

The BBR shift for the clock transition is the difference of the BBR shifts between the individual levels involved in the transition and can be written as,

$$\Delta\nu_{BBR}(4s - 3d_{\frac{5}{2}}) = \Delta\nu(3d_{\frac{5}{2}}) - \Delta\nu(4s). \quad (12)$$

Table II shows the BBR shift and scalar dipole polarizabilities of individual levels for  $4s_{\frac{1}{2}} - 3d_{\frac{5}{2}}$  clock transition of  $\text{Ca}^+$  ion. The present BBR shift is 0.367 Hz which agrees with the value of Mitroy *et al.*[31] about 0.16%, Sahoo *et al.*[32] about 0.7%, Arora *et al.*[17] about 3.3%, Champenois *et al.*[34] about 5.7% and Kajita *et al.*[35] about 8.15%. In the recent experiment, the BBR shift is 0.35(0.009) Hz at temperature  $T = 294.4 \pm 1.6$  K[36]. If we set  $T = 294.4$  K in our calculation, the BBR shift is 0.341 Hz which is within the experimental error bar.

#### C. DYNAMIC POLARIZABILITIES

##### 1. linearly polarized light

For the case of the linear polarization ( $A=0$ ), the vector polarizability does not contribute to total polarizability. The polarizability only has scalar component for state with  $j = \frac{1}{2}$ . The polarizability has scalar and tensor components for state with  $j > \frac{1}{2}$ . Supplemental Fig.I gives dynamic polarizabilities of  $4s$ ,  $4p_j$  and  $3d_j$  states for the linearly polarized light[41].

Table III lists magic wavelengths for the  $4s_{\frac{1}{2}} - 4p_{\frac{1}{2},\frac{3}{2}}$  and  $4s_{\frac{1}{2}} - 3d_{\frac{3}{2},\frac{5}{2}}$  transitions of  $\text{Ca}^+$  for the linearly polarized light. Uncertainties for all the magic wavelengths have been estimated which are similar to the estimations of Tang *et al.*[15]. For the  $4s - 4p_j$  polarizability difference, the matrix elements of  $4s - 4p_j$ ,  $4p_j - 5s$ ,  $4p_j - 3d_j$  and  $4p_j - 4d_j$  are dominant. For the  $4s - 3d_j$  polarizability difference, the matrix elements of  $4s - 4p_j$  and  $3d_j - 4p_j$  are dominant. All these matrix elements were changed by  $\pm 2\%$  and the magic wavelengths were recomputed. The magic wavelengths near 368 nm, 395 nm and 850 nm for  $4s - 4p_j$  and  $4s - 3d_j$  transitions agree with the results of available theoretical values[13, 15] excellently. The maximum difference is 0.7 nm at 850.9217 nm for  $4s - 4p_{\frac{3}{2}}$  transition. Compared to experimental value [14], the differences of magic wavelengths at 395.7958 nm

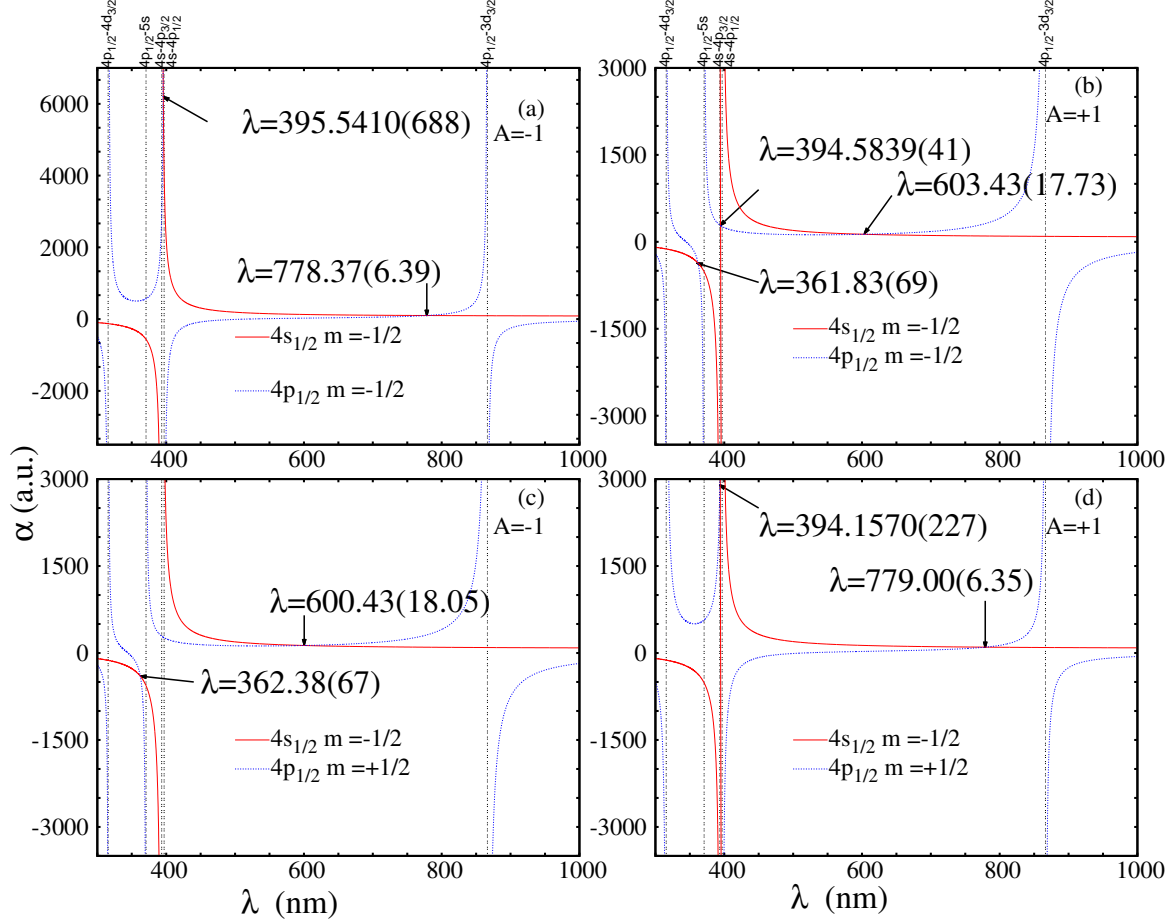


FIG. 1: (color online) Dynamic polarizabilities (in au) for the  $4s_{\frac{1}{2}m=-\frac{1}{2}}$  and  $4p_{\frac{1}{2}m=\pm\frac{1}{2}}$  states of  $\text{Ca}^+$  for the left and right handed circularly polarized light. The various magic wavelengths are identified by arrows. The vertical lines identify the resonance transition wavelengths.

and 395.7963 nm for  $4s - 3d_{\frac{5}{2}}$ , are only 0.0034 nm and 0.0027 nm, respectively. Present magic wavelengths near 691 nm, 672 nm, 687 nm, 887 nm, 1073 nm and 1307 nm for  $4s-4p_j$  and  $4s-3d_j$  transitions are in good agreement with results of Tang *et al.*[15]. The maximum difference is 0.99 nm near 1307 nm for  $4s - 3d_{\frac{3}{2}m=\frac{1}{2}}$  transition. But the results of Kaur *et al.*[13] have big differences with the present results and Tang's results [15] for these magic wavelengths, For example, the differences are 6.4 nm near 691 nm for the  $4s_{\frac{1}{2}} - 4p_{\frac{1}{2}}$  transition, 55 nm near 1307.60 nm for  $4s_{\frac{1}{2}} - 3d_{\frac{3}{2}}$  transition. Supplemental Tables III-X lists the breakdown of the polarizabilities at the magic wavelengths[41].

## 2. circularly polarized light

For the circularly polarized light, the polarizability has the scalar, vector and tensor components. The dynamic polarizability is different for each of magnetic sublevels

of the atomic state. Due to the symmetry, the dynamic polarizabilities of negative  $m$  state for  $A = -1$  will be same as positive  $m$  state for  $A = +1$ . In the following discussion, we just give the polarizabilities for the ground state  $4s_{\frac{1}{2}m=-\frac{1}{2}}$ .

Fig.1 shows the dynamic polarizabilities of the  $4s_{\frac{1}{2}m=-\frac{1}{2}}$  and  $4p_{\frac{1}{2}m=\pm\frac{1}{2}}$  states for the left and right handed circularly polarized light. In Fig. 1(a), we find that the dynamic polarizabilities of  $4s_{\frac{1}{2}m=-\frac{1}{2}}$  state have a big difference with the dynamic polarizabilities for the linearly polarized light. When the wavelength is close to  $4s - 4p_{\frac{1}{2}}$  transition wavelength,  $\alpha_{4s} \rightarrow \infty$  for linearly polarized light. However, the dynamic polarizabilities of  $4s_{\frac{1}{2}m=-\frac{1}{2}}$  state are not infinity for left handed circularly polarized light. The reason is that the  $4s - 4p_{\frac{1}{2}}$  transition has no contribution to the polarizability when the photo energy is close to the  $4s - 4p_{\frac{1}{2}}$  transition energy. The scalar and vector polarizabilities offset each other, that

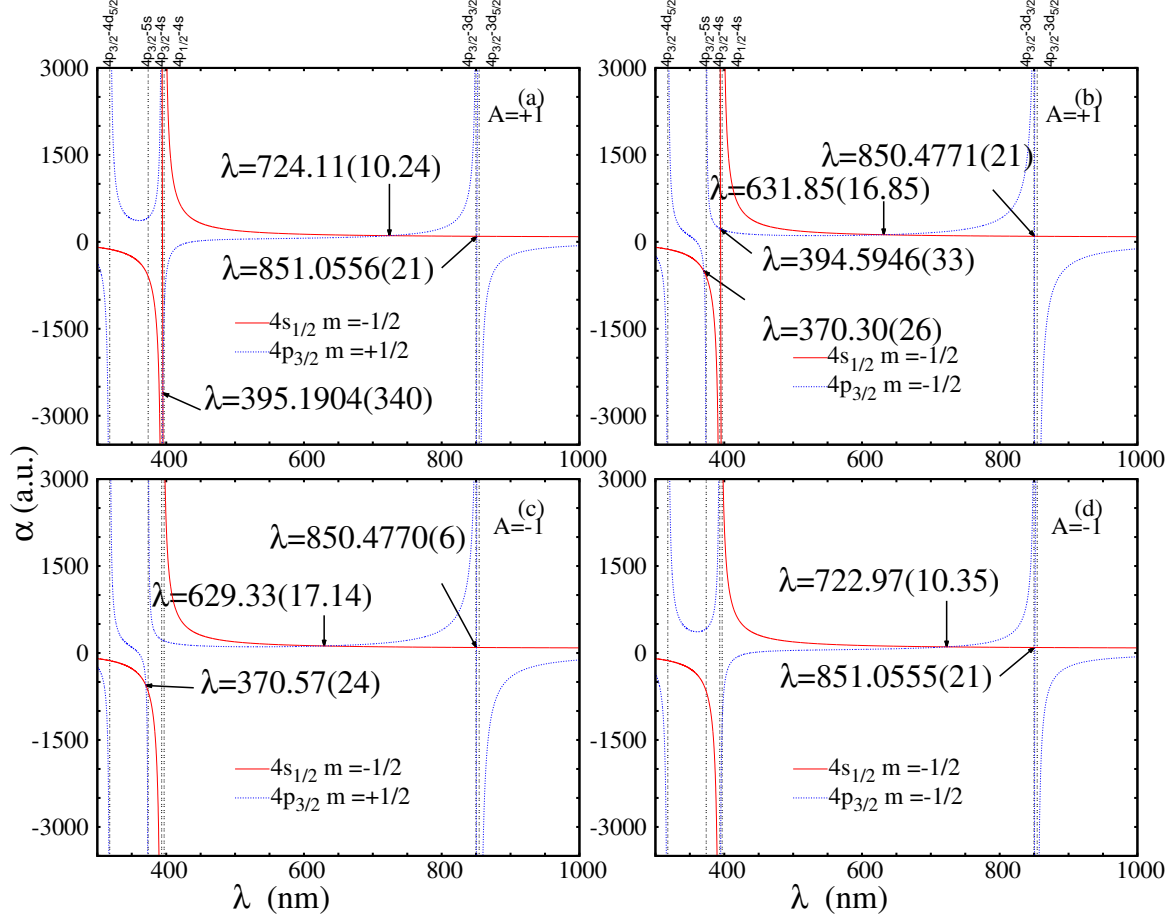


FIG. 2: (color online) Dynamic polarizabilities (in au) for the  $4s_{\frac{1}{2}}m=-\frac{1}{2}$  and  $4p_{\frac{3}{2}}m=\pm\frac{1}{2}$  states of  $\text{Ca}^+$  for the left and right handed circularly polarized light. The various magic wavelengths are identified by arrows. The vertical lines identify the resonance transition wavelengths.

is

$$\begin{aligned}
 & \lim_{\omega \rightarrow \Delta E(4s-np_{\frac{1}{2}})} \left( \frac{1}{3(2j_i+1)} |\langle \psi_{4s} || D || \psi_{np_{\frac{1}{2}}} \rangle|^2 \right. \\
 & \times \left[ \frac{1}{\Delta E_{4s-np_{\frac{1}{2}}} + \omega} + \frac{1}{\Delta E_{4s-np_{\frac{1}{2}}} - \omega} \right] \\
 & - A \frac{m_{j_i}}{2j_i} \sqrt{\frac{6j_i}{(j_i+1)(2j_i+1)}} \begin{Bmatrix} j_i & 1 & j_n \\ 1 & j_i & 1 \end{Bmatrix} \\
 & \times (-1)^{j_i+j_n+1} |\langle \psi_{4s} || D || \psi_{np_{\frac{1}{2}}} \rangle|^2 \\
 & \times \left[ \frac{1}{\Delta E_{4s-np_{\frac{1}{2}}} + \omega} - \frac{1}{\Delta E_{4s-np_{\frac{1}{2}}} - \omega} \right] \Big) \\
 & = 0.
 \end{aligned} \tag{13}$$

where,  $j_i = \frac{1}{2}$  is total angular momentum for  $4s$  state,  $j_n$  is total angular momentum for  $np_{\frac{1}{2}}$  state and  $m_{j_i} = -\frac{1}{2}$  is magnetic quantum number for  $4s$  state. Same situations also happened for  $4p_{\frac{1}{2}}m=-\frac{1}{2}$  state when the wavelength

is close to  $4p_{\frac{1}{2}} - 5s$  transition wavelength. There are two magic wavelengths for  $4s_{\frac{1}{2}}m=-\frac{1}{2} - 4p_{\frac{1}{2}}m=-\frac{1}{2}$  transition for  $A=-1$ . The first magic wavelength is 395.5410 nm which lies between  $4s - 4p_{\frac{1}{2}}$  and  $4s - 4p_{\frac{3}{2}}$  resonances energy. This magic wavelength is very close to the magic wavelength 395.1788 nm for  $4s - 4p_{\frac{1}{2}}$  transition for linearly polarized light [13, 15]. Another magic wavelength 778.37 nm occurs between  $4p_{\frac{1}{2}} - 4s$  and  $4p_{\frac{1}{2}} - 3d_{\frac{3}{2}}$  transition energy. This magic wavelength has 87 nm difference with the magic wavelength 691.24 nm of  $4s - 4p_{\frac{1}{2}}$  transition for linearly polarized light which also lies between  $4p_{\frac{1}{2}} - 4s$  and  $4p_{\frac{1}{2}} - 3d_{\frac{3}{2}}$  transitions.

Fig.1(b) gives the dynamic polarizabilities of  $4s_{\frac{1}{2}}m=-\frac{1}{2}$  and  $4p_{\frac{1}{2}}m=-\frac{1}{2}$  for right handed circularly polarized light. The change of polarizabilities of  $4s$  state is similar to linearly polarized light. Three magic wavelengths are found for  $4s_{\frac{1}{2}}m=-\frac{1}{2} - 4p_{\frac{1}{2}}m=-\frac{1}{2}$  transition. The first magic wavelength 361.83 nm occurs between the energies of the  $4p_{\frac{1}{2}} - 4d_{\frac{3}{2}}$  and the  $4p_{\frac{1}{2}} - 5s$  transitions. The second



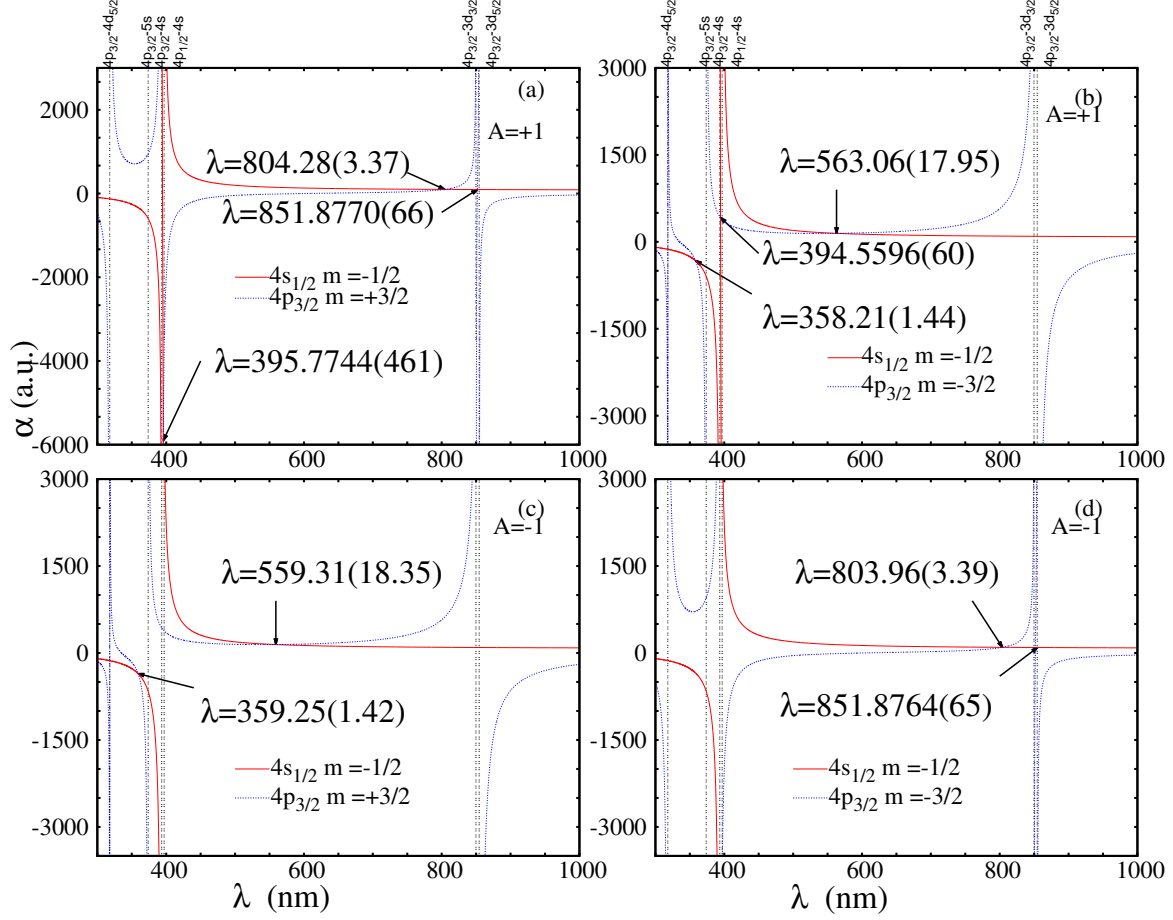


FIG. 3: (color online) Dynamic polarizabilities (in au) for the  $4s_{\frac{1}{2}m=-\frac{1}{2}}$  and  $4p_{\frac{3}{2}m=\pm\frac{3}{2}}$  states of  $\text{Ca}^+$  for the left and right handed circularly polarized light. The various magic wavelengths are identified by arrows. The vertical lines identify the resonance transition wavelengths.

magic wavelength 394.5839 nm occurs between  $4s - 4p_{\frac{1}{2}}$  and  $4s - 4p_{\frac{3}{2}}$  resonant transition. The next wavelength is located around 603 nm when the photo energy gets close to the excitation energies between the  $4p_{\frac{1}{2}} - 4s$  and  $4p_{\frac{1}{2}} - 3d_{\frac{3}{2}}$  transitions.

Fig.1(c) gives the dynamic polarizabilities of  $4s_{\frac{1}{2}m=-\frac{1}{2}}$  and  $4p_{\frac{1}{2}m=+\frac{1}{2}}$  for left handed circularly polarized light. Only two magic wavelengths 362.38 and 600.43 nm are found in the considered range of wavelength. The first one occurs between  $4p_{\frac{1}{2}} - 4d_{\frac{3}{2}}$  and  $4p_{\frac{1}{2}} - 5s$  transitions. Another one occurs when the photo energy lies between  $4p_{\frac{1}{2}} - 3d_{\frac{3}{2}}$  and  $4p_{\frac{1}{2}} - 4s$  transition energies. There is no magic wavelength between  $4s - 4p_{\frac{1}{2}}$  and  $4s - 4p_{\frac{3}{2}}$  resonant transition.

Fig.1(d) gives the dynamic polarizabilities of  $4s_{\frac{1}{2}m=-\frac{1}{2}}$  and  $4p_{\frac{1}{2}m=+\frac{1}{2}}$  for right handed circularly polarized light. Two magic wavelengths are found for  $4s_{\frac{1}{2}m=-\frac{1}{2}} - 4p_{\frac{1}{2}m=\frac{1}{2}}$  transition. The first magic wavelength is 394.1570 nm which lies between  $4s - 4p_{\frac{1}{2}}$  and  $4s - 4p_{\frac{3}{2}}$  resonant tran-

sition. The second magic wavelength is located 779.00 nm when the photo energy lies between the  $4p_{\frac{1}{2}} - 3d_{\frac{3}{2}}$  and  $4p_{\frac{1}{2}} - 4s$  transitions.

Fig.2 shows the dynamic polarizabilities of the  $4s_{\frac{1}{2}m=-\frac{1}{2}}$  and  $4p_{\frac{3}{2}m=\pm\frac{3}{2}}$  states for the left and right handed circularly polarized light. Fig.2(a) shows the dynamic polarizabilities of  $4s_{\frac{1}{2}m=-\frac{1}{2}}$  and  $4p_{\frac{3}{2}m=\frac{3}{2}}$  states for  $A=+1$ . There are three magic wavelengths in the range of 360 nm to 1000 nm for this transition. There is no magic wavelength between  $4p_{\frac{3}{2}} - 4d_{\frac{5}{2}}$  and  $4p_{\frac{3}{2}} - 5s$  transitions. The first magic wavelength 395.1904 nm lies between the  $4s - 4p_{\frac{1}{2}}$  and  $4s - 4p_{\frac{3}{2}}$  resonant transition, that just has 1.0 nm difference compared to that for the linearly polarized light. The second magic wavelength 724.11 nm lies between the  $4p_{\frac{1}{2}} - 4s$  and  $4p_{\frac{3}{2}} - 3d_{\frac{3}{2}}$  transitions, which is larger about 37 nm than the 687.51 nm for linearly polarized light. The last one 851.0556 nm is close to the magic wavelength 850.1164 nm for linearly polarized light which lies between the transition energy of  $4p_{\frac{3}{2}} - 3d_j$ .

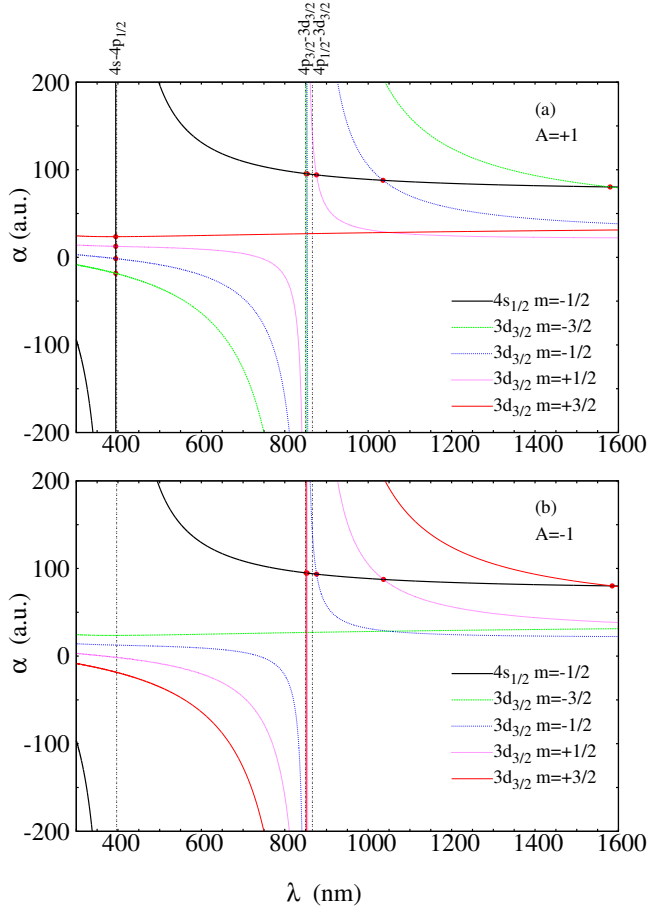


FIG. 4: (color online) Dynamic polarizabilities (in au) for the  $4s_{\frac{1}{2}} m=-\frac{1}{2}$  and  $3d_{\frac{3}{2}} m_j$  states of  $\text{Ca}^+$  for the left and right handed circularly polarized light. The various magic wavelengths are identified by red points. The vertical lines identify the resonance transition wavelengths.

Much more attentions should be paid on the magic wavelength near 851 nm, because this wavelength arises due to cancellations in the polarizabilities from two transitions of  $4p_{\frac{3}{2}} \rightarrow 3d_j$  spin-orbital splitting. From the Table XXV in Supplement[41], it can be found that the  $4s_{\frac{1}{2}} m=-\frac{1}{2}$  polarizability is dominated by  $4s_{\frac{1}{2}} - 4p_j$  transitions and the  $4p_{\frac{3}{2}} m=\frac{1}{2}$  polarizability is dominated by  $4p_{\frac{3}{2}} \rightarrow 3d_j$  transitions. Combining with the experimental matrix elements of  $4s \rightarrow 4p_j$  transitions, the measurement of this magic wavelength could be able to determine the oscillator strength ratio of  $f_{4p_{\frac{3}{2}} \rightarrow 3d_{\frac{3}{2}}} : f_{4p_{\frac{3}{2}} \rightarrow 3d_{\frac{5}{2}}}$ . Suppose that all the remaining components accuracy of  $4p_{\frac{3}{2}}$  polarizability including the  $4p_{\frac{3}{2}} \rightarrow 5s_{\frac{1}{2}}$  and  $4d_j$  contributions is 5%. Then the overall uncertainty to the polarizability is less than 1%.

The dynamic polarizabilities of  $4s_{\frac{1}{2}} m=-\frac{1}{2}$  and  $4p_{\frac{3}{2}} m=-\frac{1}{2}$  states for  $A=+1$  are shown in Fig.2(b). There are four magic wavelengths in the range of 360 nm to 1000 nm. The first magic wavelength 370.30 nm occurs when the photo energy lies between energy of  $4p_{\frac{3}{2}} - 4d_{\frac{5}{2}}$

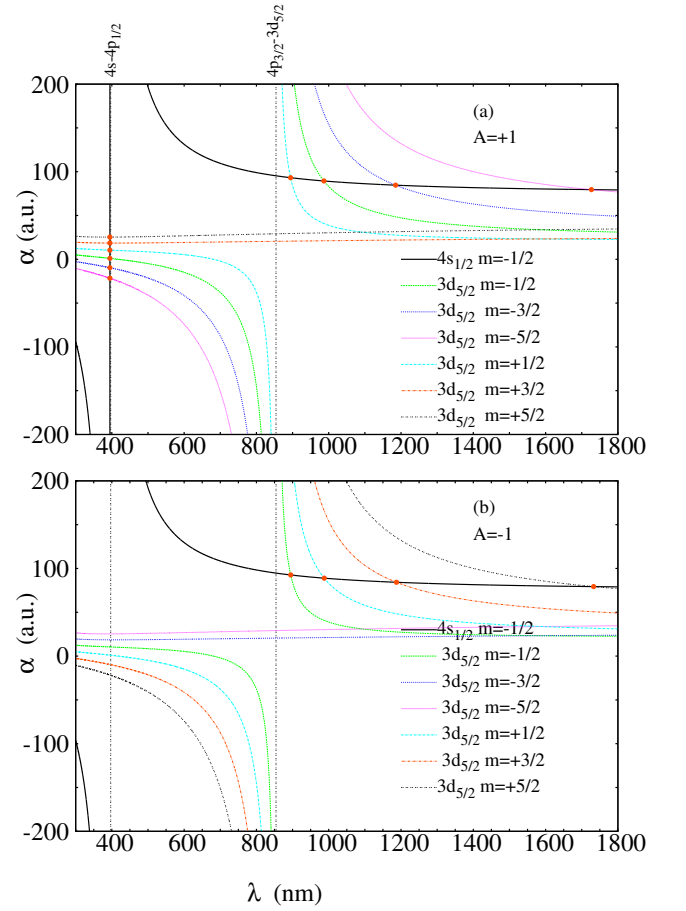


FIG. 5: (color online) Dynamic polarizabilities (in au) for the  $4s_{\frac{1}{2}} m=-\frac{1}{2}$  and  $3d_{\frac{5}{2}} m_j$  states of  $\text{Ca}^+$  for the left and right handed circularly polarized light. The various magic wavelengths are identified by red points. The vertical lines identify the resonance transition wavelengths.

and  $4p_{\frac{3}{2}} - 5s$  transitions. This magic wavelength is larger about 0.6 nm than the magic wavelength 369.65 nm for  $4s - 4p_{\frac{3}{2}} m=\frac{1}{2}$  transition for linearly polarized light, which also lies between  $4p_{\frac{3}{2}} - 4d_{\frac{5}{2}}$  and  $4p_{\frac{3}{2}} - 5s$  transitions. The second magic wavelength is 395.5946 nm which lies between the  $4s - 4p_{\frac{1}{2}}$  and  $4s - 4p_{\frac{3}{2}}$  resonant transition. The third one is 631.85 nm when photo energy lies between the  $4p_{\frac{3}{2}} - 3d_{\frac{5}{2}}$  and  $4p_{\frac{1}{2}} - 4s$  transitions. The last magic wavelength occurs 850.4771 nm which occurs between the  $4p_{\frac{3}{2}} - 3d_{\frac{3}{2}}$  and  $4p_{\frac{3}{2}} - 3d_{\frac{5}{2}}$  resonant transition. The dynamic polarizabilities of  $4s_{\frac{1}{2}} m=-\frac{1}{2}$  and  $4p_{\frac{3}{2}} m=+\frac{1}{2}$  states for  $A = -1$  are shown in Fig.2(c). Three magic wavelengths are got for the  $4s_{\frac{1}{2}} m=-\frac{1}{2} - 4p_{\frac{3}{2}} m=+\frac{1}{2}$  transition. The first one 370.57 nm lies between the  $4p_{\frac{3}{2}} - 4d_{\frac{5}{2}}$  and  $4p_{\frac{3}{2}} - 5s$  transitions. The second one 629.33 nm lies between the  $4p_{\frac{3}{2}} - 3d_{\frac{5}{2}}$  and  $4p_{\frac{1}{2}} - 4s$  transitions, that has about 58 nm difference compared to 687.51 nm for the linearly polarized light. The last one is 850.4770 nm which lies between  $4p_{\frac{3}{2}} - 4d_j$  transitions.



TABLE IV: Magic wavelengths (in nm) for the  $4s_{\frac{1}{2}m=-\frac{1}{2}} - 3d_{\frac{3}{2}m_j}$  transition of  $\text{Ca}^+$  with the circularly polarized lights.

A=-1	A=1	A=-1	A=1
$m_j = \frac{3}{2}$		$m_j = -\frac{3}{2}$	
1584.95(143.70)		1580.01(142.74)	
851.1728(42)		851.1724(42)	
	394.6315(2)		394.6394(4)
$m_j = \frac{1}{2}$		$m_j = -\frac{1}{2}$	
1036.70(20.30)		1035.46(20.15)	
853.5998(264)	876.07(2.59)	876.28(2.61)	853.5974(266)
	394.6335(1)		394.6362 (1)

TABLE V: Magic wavelengths (in nm) for the  $4s_{\frac{1}{2}m=-\frac{1}{2}} - 3d_{\frac{5}{2}m_j}$  transition of  $\text{Ca}^+$  with the circularly polarized lights.

A=-1	A=1	A=-1	A=1
$m_j = \frac{5}{2}$		$m_j = -\frac{5}{2}$	
1732.77(200.04)		1726.68(198.7)	
	394.6311(3)		394.6400(4)
$m_j = \frac{3}{2}$		$m_j = -\frac{3}{2}$	
1187.42(46.79)		1185.07(46.46)	
	394.6324(2)		394.6377(2)
$m_j = \frac{1}{2}$		$m_j = -\frac{1}{2}$	
987.60(14.87)	894.50(4.03)	894.81(4.06)	986.63(14.76)
	394.6339(1)		394.6357(1)

The dynamic polarizabilities of  $4s_{\frac{1}{2}m=-\frac{1}{2}}$  and  $4p_{\frac{3}{2}m=-\frac{1}{2}}$  states for  $A=-1$  are shown in Fig.2(d). The only two magic wavelengths are found. The first one 722.97nm lies between the  $4p_{\frac{3}{2}} - 3d_{\frac{5}{2}}$  and  $4p_{\frac{3}{2}} - 4s$  transitions. Another one 851.0555 nm occurs between the  $4p_{\frac{3}{2}} - 3d_{\frac{5}{2}}$  and  $4p_{\frac{3}{2}} - 3d_{\frac{3}{2}}$  transitions.

Fig.3 shows the dynamic polarizabilities of the  $4s_{\frac{1}{2}m=-\frac{1}{2}}$  and  $4p_{\frac{3}{2}m=\pm\frac{3}{2}}$  states for the left and right handed circularly polarized light. The dynamic polarizabilities of  $4s_{\frac{1}{2}m=-\frac{1}{2}}$  and  $4p_{\frac{3}{2}m=+\frac{3}{2}}$  states for  $A=+1$  are shown in Fig.3(a). There are three magic wavelengths in the range of 370 nm to 1000 nm. The first magic wavelength 395.7744 nm occurs when the photo energy lies between energy of  $4s - 4p_j$  resonant transitions. The second magic wavelength 804.28 nm which lies between  $4p_{\frac{3}{2}} - 4s$  and  $4p_{\frac{3}{2}} - 3d_{\frac{3}{2}}$  transitions is larger about 131 nm than 672.89 nm for the linearly polarized light. The third magic wavelength 851.8770 nm is close to the magic wavelength 850.9217 nm for the linearly polarized light. Three magic wavelengths are found for the  $4s_{\frac{1}{2}m=-\frac{1}{2}} - 4p_{\frac{3}{2}m=-\frac{3}{2}}$  transition for the right handed polarized light in Fig.3(b), that are 358.21 nm 394.5596 nm and 563.06 nm. The dynamic polarizabilities of  $4s_{\frac{1}{2}m=-\frac{1}{2}}$  and  $4p_{\frac{3}{2}m=+\frac{3}{2}}$  states for  $A=-1$  are shown in Fig.3(c). Two magic wavelengths for this transition are found at 359.25 nm and 559.31 nm. The dynamic polarizabilities of  $4s_{\frac{1}{2}m=-\frac{1}{2}}$  and  $4p_{\frac{3}{2}m=-\frac{3}{2}}$  states for  $A=-1$  are shown in Fig.3(d). Two magic wavelengths 803.96 nm and 851.8764 nm are found.

The dynamic polarizabilities of the  $4s_{\frac{1}{2}m=-\frac{1}{2}}$  and  $3d_{\frac{3}{2}m}$  states are shown in Fig.4. We also find that the dynamic polarizabilities of  $3d_{\frac{3}{2}m=\frac{3}{2}}$  state have a big difference with dynamic polarizabilities for the linearly polarized light. When the wavelength is close to  $3d_{\frac{3}{2}} - 4p_{\frac{3}{2}}$  and  $3d_{\frac{3}{2}} - 4p_{\frac{1}{2}}$  transition wavelengths,  $\alpha_{3d_{\frac{3}{2}m=\frac{3}{2}}} \rightarrow \infty$  for linearly polarized light. The dynamic polarizabilities of  $3d_{\frac{3}{2}m=\frac{3}{2}}$  state are not infinity for the right handed circularly polarized light. The  $3d_{\frac{3}{2}} - 4p_{\frac{1}{2}}$  or  $3d_{\frac{3}{2}} - 4p_{\frac{3}{2}}$  transition have no contribution to the polarizability when the photo energy is close to their transition energy. The scalar, vector and tensor polarizabilities offset each other,

$$\begin{aligned}
& \lim_{\omega \rightarrow \Delta E(3d_{\frac{3}{2}} - np_j)} \left( \frac{1}{3(2j_i + 1)} |\langle \psi_{3d_{\frac{3}{2}}} \| D \| \psi_{np_j} \rangle|^2 \right. \\
& \times \left[ \frac{1}{\Delta E_{3d_{\frac{3}{2}} - np_j} + \omega} + \frac{1}{\Delta E_{3d_{\frac{3}{2}} - np_j} - \omega} \right] \\
& - A \frac{m_{j_i}}{2j_i} \sqrt{\frac{6j_i}{(j_i + 1)(2j_i + 1)}} \left\{ \begin{matrix} j_i & 1 & j_n \\ 1 & j_i & 1 \end{matrix} \right\} \\
& \times (-1)^{j_i + j_n + 1} |\langle \psi_{4s} \| D \| \psi_{np_j} \rangle|^2 \\
& \times \left[ \frac{1}{\Delta E_{3d_{\frac{3}{2}} - np_j} + \omega} - \frac{1}{\Delta E_{3d_{\frac{3}{2}} - np_j} - \omega} \right] \\
& - \frac{3m_{j_i}^2 - j_i(j_i + 1)}{2j_i(2j_i - 1)} \times (-2) \sqrt{\frac{5j_i(2j_i - 1)}{6(j_i + 1)(2j_i + 1)(2j_i + 3)}} \\
& \times \left\{ \begin{matrix} j_i & 1 & j_n \\ 1 & j_i & 2 \end{matrix} \right\} \times (-1)^{j_i + j_n + 1} |\langle \psi_{3d_{\frac{3}{2}}} \| D \| \psi_{np_j} \rangle|^2 \\
& \times \left[ \frac{1}{\Delta E_{3d_{\frac{3}{2}} - np_j} + \omega} + \frac{1}{\Delta E_{3d_{\frac{3}{2}} - np_j} - \omega} \right] \Big) \\
& = 0.
\end{aligned} \tag{14}$$

where,  $j_i = \frac{3}{2}$  is total angular momentum for  $3d_{\frac{3}{2}}$  state,  $j_n = \frac{1}{2}, \frac{3}{2}$  is total angular momentum for  $np_j$  state and  $m_{j_i} = +\frac{3}{2}$  is magnetic quantum number for  $3d_{\frac{3}{2}}$  state. The magic wavelengths are listed in Table IV. It can be found that there are two or three magic wavelength for each of  $4s_{\frac{1}{2}m=-\frac{1}{2}} - 3d_{\frac{3}{2},m}$  transitions. It should be noted that wavelength near 394.6 nm lies between the  $4s - 4p_j$  resonant transitions which is smaller about 1 nm than 394.79 nm of  $4s - 3d_{\frac{3}{2}m}$  transition for the linearly polarized light. The measurement of magic wavelength near 394.6 nm can be use to a further check the ratio of the  $f_{4s-4p_j}$  oscillator strength. As mentioned before, the measurement of magic wavelength near 850 nm for  $4s_{\frac{1}{2}m=-\frac{1}{2}} - 3d_{\frac{3}{2},m=\pm\frac{1}{2}}$  is able to determine the oscillator strength ratio of  $f_{4p_{\frac{3}{2}} \rightarrow 3d_{\frac{3}{2}}} : f_{4p_{\frac{3}{2}} \rightarrow 3d_{\frac{5}{2}}}$ .

The dynamic polarizabilities of the  $4s_{\frac{1}{2}m=-\frac{1}{2}}$  and  $3d_{\frac{5}{2},m}$  states are shown in Fig.5. Table V gives the magic wavelengths of  $4s_{\frac{1}{2}m=-\frac{1}{2}} - 3d_{\frac{5}{2},m}$  transitions. There are only one or two magic wavelength for each of  $4s_{\frac{1}{2}m=-\frac{1}{2}} - 3d_{\frac{5}{2},m}$  transition. Similar to the experiment of Liu *et*

*al.*[14], the measurement of magic wavelength near 394.6 nm can be used to further check the ratio of the  $f_{4s-4p_j}$  oscillator strength.

#### IV. CONCLUSIONS

The energy levels, electric dipole matrix elements and static polarizabilities are calculated using RCICP procedure. The polarizabilities for the  $4s$ ,  $4p_j$  and  $3d_j$  states agree with the available theoretical and experimental results very well. The BBR shift for the  $4s - 3d_{\frac{5}{2}}$  clock transition is also determined and the present result is within the recent experimental error bar[36].

The dynamic dipole polarizabilities of the  $4s$ ,  $4p_j$  and  $3d_j$  states of  $\text{Ca}^+$  ion are calculated for the linearly and circularly polarized light. The magic wavelengths for each of magnetic sublevels of  $4s - 4p_j$  and  $4s - 3d_j$  transitions are determined. The magic wavelengths for the linearly polarized light agree with the available theoret-

ical results[13, 15] excellently. The magic wavelengths for the circularly polarized light have very big difference with those for linearly polarized light. Some additional magic wavelengths are found for circularly polarized light. We recommend that the measurement of the magic wavelength near 850 nm of  $4s - 4p_{\frac{3}{2}, m=\pm\frac{3}{2}, \pm\frac{1}{2}}$  could be able to determine the oscillator strength ratio of  $f_{4p_{\frac{3}{2}} \rightarrow 3d_{\frac{3}{2}}}$  and  $f_{4p_{\frac{3}{2}} \rightarrow 3d_{\frac{5}{2}}}$ .

#### V. ACKNOWLEDGMENTS

The work of JJ was supported by National Natural Science Foundation of China (NSFC) (Grants No.11564036). The work of LYX was supported by NSFC(Grants No. U1331122). The work of DHZ was supported by NSFC (Grants No. 11464042, U1330117). The work of CZD was supported by NSFC (Grants No.11274254, U1332206).

- 
- [1] J. Ye, D. W. Vernooy, and H. J. Kimble, Phys. Rev. Lett. **83**, 4987 (1999).
  - [2] H. Katori, T. Ido, and M. Kuwata-Gonokami, J. Phys. Soc. Japan **68**, 2479 (1999).
  - [3] M. Takamoto and H. Katori, Phys. Rev. Lett. **91**, 223001 (2003).
  - [4] A. Bauch, Meas. Sci. Technol. **14**, 1159 (2003).
  - [5] P. Gill, G. P. Barwood, H. A. Klein, G. Huang, S. A. Webster, P. J. Blythe, K. Hosaka, S. N. Lea, and H. S. Margolis, Meas. Sci. Technol. **14**, 1174 (2003).
  - [6] P. Gill, Metrologia **42**, S125 (2005).
  - [7] L. Lorini, N. Ashby, A. Brusch, S. Diddams, R. Drullinger, E. Eason, T. Fortier, P. Hastings, T. Heavner, D. Hume, et al., Eur. Phys. J. Special Topics **163**, 19 (2008).
  - [8] P. Gill, Royal Soc. of London Phil. Trans. Series A **369**, 4109 (2011).
  - [9] G. Kirchmair, J. Benhelm, F. Zähringer, R. Gerritsma, C. F. Roos, and R. Blatt, Phys. Rev. A **79**, 020304 (2009).
  - [10] B. K. Sahoo and B. Arora, Phys. Rev. A **87**, 023402 (2013).
  - [11] G. Wilpers, C. W. Oates, S. A. Diddams, A. Bartels, T. M. Fortier, W. H. Oskay, J. C. Bergquist, S. R. Jefferts, T. P. Heavner, T. E. Parker, et al., Metrologia **44**, 146 (2007).
  - [12] A. D. Ludlow, T. Zelevinsky, G. K. Campbell, S. Blatt, M. M. Boyd, M. H. de Miranda, M. J. Martin, J. W. Thomsen, S. M. Foreman, and J. Ye, Science **319**, 1805 (2008).
  - [13] J. Kaur, S. Singh, B. Arora, and B. K. Sahoo, Phys. Rev. A **92**, 031402 (2015).
  - [14] P.-L. Liu, Y. Huang, W. Bian, H. Shao, H. Guan, Y.-B. Tang, C.-B. Li, J. Mitroy, and K.-L. Gao, Phys. Rev. Lett. **114**, 223001 (2015).
  - [15] Y.-B. Tang, H.-X. Qiao, T.-Y. Shi, and J. Mitroy, Phys. Rev. A **87**, 042517 (2013).
  - [16] N. Lundblad, M. Schlosser, and J. V. Porto, Phys. Rev. A **81**, 031611 (2010).
  - [17] B. Arora, M. S. Safronova, and C. W. Clark, Phys. Rev. A **76**, 064501 (2007).
  - [18] S. Singh, B. K. Sahoo, and B. Arora, Phys. Rev. A **94**, 023418 (2016).
  - [19] B. Arora and B. K. Sahoo, Phys. Rev. A **86**, 033416 (2012).
  - [20] S. Singh, B. K. Sahoo, and B. Arora, Phys. Rev. A **93**, 063422 (2016).
  - [21] S. Singh, K. Kaur, B. K. Sahoo, and B. Arora, Journal of Physics B Atomic Molecular Physics **49** (2016).
  - [22] F. Le Kien, P. Schneeweiss, and A. Rauschenbeutel, The European Physical Journal D **67**, 92 (2013), ISSN 1434-6060.
  - [23] K. L. Gao, Science Bulletin **58**, 853 (2013).
  - [24] Y. Huang, J. Cao, P. Liu, K. Liang, B. Ou, H. Guan, X. Huang, T. Li, and K. Gao, Phys. Rev. A **85**, 030503 (2012).
  - [25] C. Degenhardt, H. Stoeck, U. Sterr, F. Riehle, and C. Lisdat, Phys. Rev. A **70**, 023414 (2004).
  - [26] M. Chwalla, J. Benhelm, K. Kim, G. Kirchmair, T. Monz, M. Riebe, P. Schindler, A. S. Villar, W. Hänsel, C. F. Roos, et al., Phys. Rev. Lett. **102**, 023002 (2009).
  - [27] P. Zhang, J. Cao, H. Lin Shu, J. Bo Yuan, J. Juan Shang, K. Feng Cui, S. Jia Chao, S. Mao Wang, D. Xin Liu, and X. Ren Huang, Journal of Physics B: Atomic, Molecular and Optical Physics **50**, 015002 (2017).
  - [28] H. Hffner, C. Roos, and R. Blatt, Physics Reports **469**, 155 (2008).
  - [29] Y. Huang, H. Guan, P. Liu, W. Bian, L. Ma, K. Liang, T. Li, and K. Gao, Phys. Rev. Lett. **116**, 013001 (2016).
  - [30] M. S. Safronova and U. I. Safronova, Phys. Rev. A **83**, 012503 (2011).
  - [31] J. Mitroy, J. Y. Zhang, M. W. J. Bromley, and S. I. Young, Phys. Rev. A **78**, 012715 (2008).
  - [32] B. K. Sahoo, B. P. Das, and D. Mukherjee, Phys. Rev.

- A **79**, 052511 (2009).
- [33] E. S. Chang, Journal of Physics B: Atomic and Molecular Physics **16**, L539 (1983).
  - [34] C. Champenois, M. Knoop, M. Houssin, G. Hagel, M. Vedel, and F. Vedel, ArXiv Physics e-prints (2005), physics/0511089.
  - [35] M. Kajita, Y. Li, K. Matsubara, K. Hayasaka, and M. Hosokawa, Phys. Rev. A **72**, 043404 (2005).
  - [36] H. Guan, Y. Huang, and K.-L. Gao, Scientia Sinica, Physica, Mechanica Astronomica **7**, 006 (2016).
  - [37] Y. Huang, J. Cao, P. Liu, K. Liang, B. Ou, H. Guan, X. Huang, T. Li, and K. Gao, Phys. Rev. A **85**, 030503 (2012).
  - [38] Y. Huang, Q. Liu, J. Cao, B. Ou, P. Liu, H. Guan, X. Huang, and K. Gao, Phys. Rev. A **84**, 053841 (2011).
  - [39] J. Jiang, J. Mitroy, Y. Cheng, and M. W. J. Bromley, Phys. Rev. A **94**, 062514 (2016).
  - [40] M. S. Safronova and U. I. Safronova, Phys. Rev. A **83**, 012503 (2011).
  - [41] See Supplemental Material at <http://XXXXXXXX> for additional tables of energy levels and matrix elements and breakdowns of polarizabilities at the magic wavelengths. (???)
  - [42] N. L. Manakov, V. D. Ovsiannikov, and L. P. Rapoport, Physics Reports **141**, 320 (1986).
  - [43] K. Beloy, Ph. D thesis, University of Nevada, Reno (2009).
  - [44] S. G. Porsev and A. Derevianko, Phys. Rev. A **74**, 020502 (2006).